JOURNAL OF GUIDANCE, CONTROL, AND DYNAMICS
Vol. 28, No. 6, November–December 2005

Fuzzy Gain Scheduling for Flutter Suppression in an Unmanned Aerial Vehicle

Ellen Applebaum,* Joseph Ben-Asher,† and Tanchum Weller‡
Technion—Israel Institute of Technology, 32000 Haifa, Israel

The active flutter suppression of the flexible modes of a generic model of an unmanned aerial vehicle that exhibits open-loop nonminimum phase behavior and three flutter mechanisms is investigated. A fuzzy gain scheduler interpolates plant models, state feedback, and observer gains based on an exogenous input velocity that is frozen in time. The novelty of the approach rests on the fuzzy interpolation of high-order models and on the method of gain table construction. Closed-loop stability over a wide range of velocities is demonstrated via time simulations for both linear time-invariant plant models and their fuzzy approximations. The fuzzy gain scheduling algorithm demonstrates stronger stability characteristics and generalization capabilities over pointwise synthesized linear quadratic Gaussian controllers, reduced-order controllers, and recurrent neural networks. The resultant global linear controller extends the flutter boundary to a velocity approximately 60% higher than the first open-loop flutter onset speed.

Nomenclature

$A_{(\,)}, B_{(\,)}, C_{(\,)}$	=	aeroservoelastic state-space matrices
A^d, B^d, C^d, K^d, L^d	=	interpolated plant matrices for fixed velocity v^d
$A_{v_p}, B_{v_p}, C_{v_p} K_{v_p}, L_{v_p}$	=	linguistic labels for pth fuzzy rule consequent
$\boldsymbol{e}$	=	state estimation error vector
$\mathcal{F}(s)$	=	fuzzy regulator transfer function
$G_{(\cdot)}$	=	augmented closed-loop state-space matrix
I, I_{39}	=	39th-order identity matrix
J	=	quadratic cost function
$K_{(\,)}, L_{(\,)}$	=	state feedback and observer gains
n	=	number of gain scheduled nominal velocities
Q, R_c, N_c, N_f	=	weighting parameters
R	=	number of nominal linear time-invariant models
$\Re(z)$	=	real-part complex eigenvalue
s	=	Laplace transform variable
t	=	time
u	=	control deflection command input
V_F	=	flutter speed
V_f	=	joint correlation noise matrix
V_p	=	linguistic label for pth fuzzy rule premise
V_s, V_u, V_t	=	stable, unstable, and transitional velocity sets
v	=	flight velocity scheduling variable
v^d	=	frozen exogenous input velocity
W	=	weighting matrix for quadratic cost function
$\boldsymbol{x}, \boldsymbol{y}$	=	vectors of state and output measurements
$x_1, \ldots, x_{15}$	=	generalized flexible structural displacement modes
$x_{16}, \ldots, x_{30}$	=	generalized structural velocities
$\hat{\boldsymbol{x}}, \hat{\boldsymbol{y}}$	=	estimated system states, output measurements
$Y(\,)$	=	simulated output response accelerometer reading
α	=	prescribed degree of stability
$\delta, \dot{\delta}, \ddot{\delta}$	=	control surface deflections
ζ	=	damping ratio
θ	=	measurement noise
$\mu_p(v^d)$	=	pth fuzzy rule's premise value
μ_{RMSE}	=	mean root mean square error
ν	=	white Gaussian process noise
$\boldsymbol{\xi}$	=	normalized weight vector
$\xi_p(v^d)$	=	normalized weight for pth fuzzy rule
$\xi_1, \ldots, \xi_R$	=	components of normalized weight vector
ω	=	flutter frequency

Subscripts

a	=	augmented closed-loop system
c	=	control weighting factor
F	=	flutter speed
f	=	weighting factor for noise correlation function
p	=	index to nominal state-space model and fuzzy rule
s	=	stable nominal velocities
u	=	unstable nominal velocities
v_p	=	variable index to pth fuzzy rule

Superscripts

d	=	resultant interpolated value for fixed velocity v^d
T	=	transpose

Received 4 August 2004; revision received 12 February 2005; accepted for publication 15 February 2005.

*Research Scientist, Faculty of Aerospace Engineering.
†Associate Professor, Faculty of Aerospace Engineering. Associate Fellow AIAA.
‡Professor, Faculty of Aerospace Engineering. Associate Fellow AIAA.

Introduction

DURING the past several years, flutter suppression techniques have been actively investigated on the benchmark active control technology (BACT) wind-tunnel model developed by NASA Langley Research Center.[1–6] The BACT exhibits classical flutter instability at transonic speeds and has provided a testbed for the development and testing of passivity-based robust control, linear parameter varying gain scheduling control, H-infinity, μ-synthesis generalized predictive control, full-order and reduced-order linear quadratic Gaussian (LQG), and others. The body of flutter suppression techniques developed for the BACT model is based on a system that can be effectively reduced to a low-order state-space model. The open-loop BACT model has one flutter mechanism and is stable below the classical flutter boundary and unstable above.[2]

Recently, alternative methods for achieving flutter suppression in high-order nonminimum phase systems that exhibit three flutter mechanisms have been developed. These control strategies include gain scheduling techniques for interpolating between linear time-invariant controllers,[5,7–10] the construction of a single LQG regulator satisfying a prescribed degree of stability (PDS) criterion,[11,12]

and adaptive recurrent neural networks.[13] In the case of gain scheduling, linear matrix inequalities (LMIs) techniques have generally been applied for gain construction.[5,7,9,10] LMI techniques have been used effectively in low-order systems for constructing controller and observer gains that guarantee global stability. As the number of operating points increase, however, even in the regulation of a low-order dynamic model, it becomes more difficult to find a solution satisfying LMI modeling criteria.[9] For the high-order unmanned aerial vehicle (UAV) model under investigation, the large condition number of state-space linear time-invariant (LTI) matrices has led to infeasible or poorly scaled solutions of the LMI Lyapunov inequalities. In the case of the single, full-order LQG-PDS controller, robust performance could not be achieved for velocities slightly lower than the maximum speed about which the controller was synthesized.[11] Studies report the construction of a reduced-order LQG controller that demonstrates robust stabilization with respect to flight velocity for a specific high-order generic UAV model with a mechanical servo aileron input.[11] The LQG design criteria are model specific, and least stable eigenvalues remain close to zero. Studies report that adaptive predictive neural networks achieve a limited, nonrobust, flutter suppression envelope for a single flutter mechanism and require extensive experimentation for design of a network architecture and topology.[13]

Fuzzy gain scheduling (FGS) has been used in a variety of contexts requiring interpolation of system parameters based on independent scheduling variables. In guidance control design, adaptive FGS has been used to modify the parameters of a dynamic controller using a fuzzy logic design embedded into the architecture of a neural network.[10] In flight control, FGS has been used to construct an approximate model of aircraft dynamics and produce a control law with interpolated feedback and filter gains.[9] For active flutter suppression, the fuzzy gain scheduler approximates UAV aeroservoelastic equations, state feedback, and observer gains. Moreover, it can be shown that the fuzzy gain scheduler interpolates the state feedback and observer gains as continuous functions of the scheduling variable that is the exogenous input velocity.[14] For nonminimum phase systems, FGS has the advantage over direct and indirect methods of adaptive control. The fuzzy gain scheduled control law does not require inversion of nonminimum phase transfer functions, which would result in right-hand-side poles, nor the creation of certainty equivalent control laws to guarantee the stability of internal dynamics.[15,16]

This study describes a novel approach to active flutter suppression in a generic high-order nonminimum phase UAV system. Fuzzy interpolation of gains and high-order linear models, combined with LQG synthesis, has been successfully applied to several UAV models with piezoelectric lead zirconate titanate (PZT) or mechanical aileron servo input.[14] Stability criteria were established using two-norm differences between state-space models and their fuzzy gain scheduled approximations. The next section provides a mathematical model of the generic UAV system. Subsequent sections describe the architecture of the Takagi–Sugeno model for FGS, the construction of the augmented closed-loop system using fuzzy observers, the construction of the gain scheduler, and simulations of the fuzzy gain scheduled response characteristics. The MATLAB® Control Systems Toolbox and Robust Control Toolbox[17,18] were used in the construction and operation of the fuzzy gain scheduler.

Mathematical Model of Generic UAV System

The problem addressed in this research is the regulation via output feedback of the flexible modes of a generic high-order nonminimum phase aeroservoelastic UAV model designed to operate at sea level over an entire range of its flight velocity envelope. State-space open-loop aeroelastic coefficient matrices, parameterized by velocity and velocity squared, were constructed in Refs. 19 and 20 using rational approximations[21] and the NASTRAN finite element software package. The 39th-order UAV model consists of 15 generalized flexible structural displacement modes, $x_1, \ldots, x_{15}$; 15 generalized structural velocities, $x_{16}, \ldots, x_{30}$; an aerodynamic vector of six augmented states; and the third-order servomechanism. The third-order servomechanism consists of actuator states δ, $\dot{\delta}$, and $\ddot{\delta}$. The dynamic

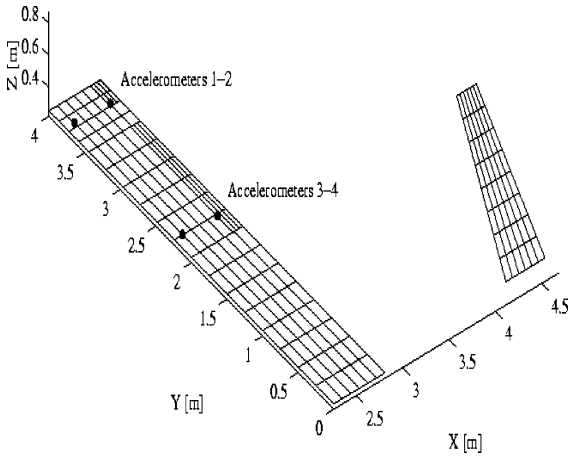

Fig. 1 UAV aerodynamic model with PZT aileron.

model of the actuator driving the control surface is described by a transfer function with three poles and no zeros. As a result of this order difference, δ, $\dot{\delta}$, and $\ddot{\delta}$ can be defined as independent states in the actuator state-space model and can be used directly as inputs to state-space open-loop aeroelastic equations of motion and in connection with acceleration sensors.[22] A complete description of the derivation of the aeroservoelastic (ASE) equations for the generic UAV model can be found in Refs. 19 and 22.

The modeling, analysis, and control of flutter is based on the aeroelastic analysis using state-space formulation. The result is the ASE plant equation

$$\dot{\boldsymbol{x}} = A\boldsymbol{x} + Bu \tag{1}$$

$$\boldsymbol{y} = C\boldsymbol{x} \tag{2}$$

The ASE model does not contain input noise. As a consequence of the embedding of actuator states in the ASE model, the vector $\boldsymbol{y}$ of sensor signals does not require a feedthrough D matrix in Eq. (2) (Ref. 22).

Figure 1 shows the UAV aerodynamic model with the PZT aileron developed in Refs. 19 and 20. The model consists of seven aerodynamic panels representing the control surface, the four parts of the wing, the aileron, and the tail. Figure 1 shows the locations of the four accelerometers that have been used for subsequent ASE analysis. The control surface located in the upper-left wing-tip trailing-edge area of Fig. 1, adjacent to accelerometers 1 and 2, contains patches of PZT layers. The control surface is deflected by a voltage command that expands the upper patch and contracts the lower one as described in Refs. 19 and 20. Open-loop flutter analysis was conducted using state-space ASE methods and frequency domain (NASTRAN) methods.[19] The results of both methods were strongly correlated and yielded three flutter mechanisms at elastic modes 5, 6, and 7. The flutter mechanisms for these modes are 1) fore and aft and torsion, 2) first bending and torsion, and 3) second bending and torsion.

Table 1 presents a comparison of the flutter parameters of the open-loop UAV with balanced aileron (without PZT control patches), using NASTRAN and ASE methods, with those of the PZT UAV model that were derived using the state-space models of the ASE plant and the numerically simulated fuzzy gain scheduler. Table 1 is an extension of Table 4.1 in Ref. 19. The three flutter parameters as listed in Table 1 are 1) mode, 2) flutter onset speed, and 3) flutter frequency. The flutter onset speed indicates the speed for which a mode's real-part eigenvalue crosses, for the first time, the imaginary axis and, thus, moves from its negative (stable) to positive (unstable) direction.

Numerical simulations of fuzzy interpolated open-loop plant models were run at discrete velocities. Based on these simulations, the first flutter onset speed occurs when elastic mode 7 becomes unstable at approximately 59 m/s. The first flutter mechanism produced by coupling between the second bending and torsion occurs for eigenvalue pair $0.026 \pm 108.86i$ and a damping ratio $\zeta = -0.0002$.

Table 1 Comparison of flutter onset parameters[a]

	NASTRAN		ASE		FGS		
Mode	v, m/s	ω, Hz	v, m/s	ω, Hz	v, m/s	ω, Hz	Flutter mechanism
7	59.01	17.47	59.54	17.25	59	17.33	Second bending and torsion
5	77.87	10.19	76.48	10.17	76.25	10.04	Fore and aft and torsion
6	77.19	13.46	77.22	13.41	78	12.4	First bending and torsion

[a]Open-loop flutter parameters.

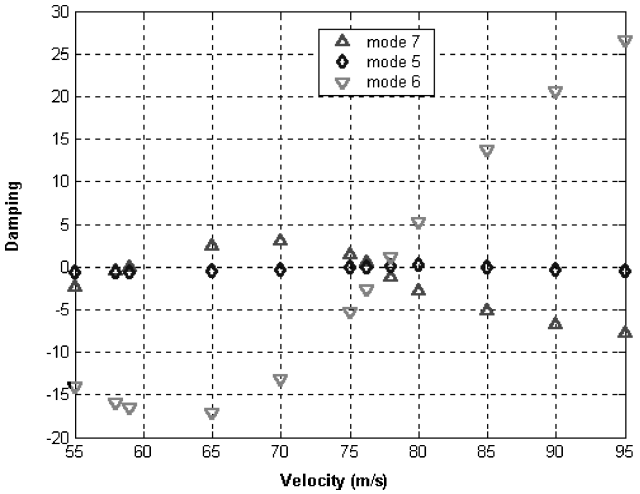

Fig. 2 Damping a for flutter onset modes.

The second flutter onset produced by coupling between for-and-aft and torsion occurs at approximately 76.25 m/s at mode 5 for eigenvalue pair $0.0029 \pm 63.08i$ and damping ratio $\zeta = -0.00005$. The third flutter onset for the flutter mechanism produced by coupling between the first bending and torsion occurs at approximately 78 m/s at mode 6 for eigenvalue pair $1.0975 \pm 78.077i$ and a damping ratio $\zeta = -0.014$. These three numerically simulated flutter onset speeds correspond very closely with the NASTRAN and state-space ASE flutter analyses of a balanced aileron UAV configuration without PZT control patches as reported in Ref. 19.

Figure 2 shows the real-part (damping) component $\Re(z) = a$ of modes 5, 6, and 7 over the velocity range between 55 and 95 m/s. By convention, positive damping indicates how much damping needs to be added to insure the mode's stability. The damping for mode 7 turns positive at 59 m/s and continues to move in the positive direction until 70 m/s. It begins to decrease and turn negative at approximately 76.25 m/s and continues to move in the negative stable direction at higher velocities. Mode 5 damping turns positive at approximately 76.25 m/s and continues to move in the positive unstable direction until approximately 80 m/s. Damping for mode 5 then begins to move in the negative stable direction, where it remains for subsequent higher velocities. Mode 6 exhibits the most critical flutter mechanism. Damping for mode 6 turns positive at approximately 78 m/s, monotonically increases, and remains unstable for all higher velocities.

FGS Architecture

FGS is a model-based fuzzy control technique that interpolates between known nominal linear plant models to construct an approximate model between nominal operating conditions. In this scheme, it is assumed that for a plant that does not belong to a predefined set of R nominal linear plant models, an approximating description (by means of fuzzy interpolation) of the plant can be derived without the necessity of further linearization. This assumption is critical for the UAV system where in real-time operation the exact description of the plant may be unknown and the approximate plant model would be used in the construction of fuzzy observers and output feedback gains.

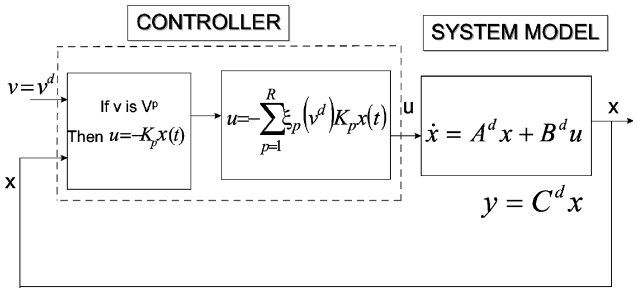

Fig. 3 TS fuzzy logic system for gain scheduling.

The functional description of FGS is derived from a set of fuzzy rules that represent a class of functional fuzzy logic systems known as Takagi–Sugeno (TS) fuzzy systems.[23] A TS fuzzy system can be thought of as a nonlinear interpolator between R nominal linear systems. The pth fuzzy system rule models the plant dynamics of Eq. (1) for the pth nominal LTI plant model:

If v is V_p, then

$$\dot{\boldsymbol{x}}_{v_p(t)} = A_{v_p}\boldsymbol{x}(t) + B_{v_p}u(t) \tag{3}$$

If v is V_p then

$$\boldsymbol{y} = C_{v_p}\boldsymbol{x}(t) \tag{4}$$

Corresponding to distinct nominal values v_p of flight velocity is the set of coefficient matrices $A(v_p)$, $B(v_p)$, and $C(v_p)$ for $p = 1, \ldots, R$. The coefficient matrices compose the LTI consequents of the pth fuzzy rule. The antecedent of the pth fuzzy rule is represented by a fuzzy membership function $\mu_p(v^d)$, which describes the degree to which a fixed velocity v^d is represented by the nominal velocity V_p. The membership function μ_p is a functional representation of V_p as a fuzzy set. The antecedent fuzzy membership function also represents the strength of a rule's firing for a fixed velocity v^d. During operation of the TS gain scheduler, the strength of rule firings over all fuzzy rules is a normalized weight vector defined by the following operator:

$$\boldsymbol{\xi}^T = [\xi_1, \ldots, \xi_R] = \left[1 \Big/ \sum_{p=1}^{R} \mu_p\right][\mu_1, \ldots, \mu_R]$$

$$\sum_{p=1}^{R} \xi_p = 1, \qquad \xi_p \geq 0 \tag{5}$$

For a fixed velocity v^d the pth fuzzy rule is said to fire when $\xi_p(v^d) > 0$.

Figure 3 shows the TS fuzzy logic control architecture for a full-state feedback controller for which all states are available. The system model represents the interpolated open-loop plant equation,

$$\dot{\boldsymbol{x}}(t) = \left\{\sum_{p=1}^{R} \xi_p(v^d)[A_p\boldsymbol{x}(t) + B_p u(t)]\right\} \tag{6}$$

$$= \left[\sum_{p=1}^{R} A_p\xi_p(v^d)\right]\boldsymbol{x}(t) + \left[\sum_{p=1}^{R} B_p\xi_p(v^d)\right]u(t) \tag{7}$$

When the following substitutions are made for a fixed flight velocity v^d,

$$A^d = \sum_{p=1}^{R} \xi_p(v^d) A_p \tag{8}$$

$$B^d = \sum_{p=1}^{R} \xi_p(v^d) B_p \tag{9}$$

the system model equation becomes

$$\dot{\boldsymbol{x}}(t) = A^d \boldsymbol{x}(t) + B^d u(t) \tag{10}$$

The matrices A^d and B^d are weighted averages of R linear models. The interpolated output vector $\boldsymbol{y}$ as a function of the state vector $\boldsymbol{x}(t)$ is computed as

$$\boldsymbol{y} = \sum_{p=1}^{R} \xi_p(v^d) C_p \boldsymbol{x}(t) \tag{11}$$

Associated with the pth nominal plant model is a fuzzy control rule:

If v is V_p then

$$u = -K_p \boldsymbol{x}(t) \tag{12}$$

The consequent of the pth fuzzy control rule, $u = -K_p \boldsymbol{x}(t)$, is the control law for stabilization of the pth nominal plant model whose state feedback gain matrix is K_p. The controller, shown in Fig. 3, is defined by a set of R fuzzy control rules, one for each nominal velocity-gain pair $[V_p, K_p]$, $p = 1, \ldots, R$, and by a TS fuzzy control law. The TS fuzzy control law is computed as a weighted sum of the consequents of the R fuzzy control rules

$$u = -\sum_{p=1}^{R} \xi_p(v^d) K_p \boldsymbol{x}(t) \tag{13}$$

The control procedure assumes the slowly time-varying nature of the scheduling parameter relative to the dynamic process under control. For the UAV system, it is reasonable to assume that flight velocity is frozen in time for the duration of time required for the stabilization of the ASE model. As a result of the fixed flight velocity v^d, interpolation is linear with respect to constant plant coefficient matrices and controller gains for both the open-loop system equation (7) and the control law (13). When the control law (13) is substituted into Eq. (7), the closed-loop interpolated system is formulated as

$$\dot{\boldsymbol{x}} = \left\{ \sum_{p=1}^{R} A_p \xi_p(v^d) + \left[\sum_{p=1}^{R} B_p \xi_p(v^d) \right] \left[-\sum_{q=1}^{R} K_q \xi_q(v^d) \right] \right\} \boldsymbol{x}(t) \tag{14}$$

$$= (A^d - B^d K^d) \boldsymbol{x}(t) \tag{15}$$

$$\boldsymbol{y} = C^d \boldsymbol{x}(t) \tag{16}$$

where

$$K^d = \sum_{q=1}^{R} K_q \xi_q(v^d) \tag{17}$$

$$C^d = \sum_{p=1}^{R} C_p \xi_p(v^d) \tag{18}$$

Construction of Fuzzy Observers

In practical applications, the states of the system are unknown, and output response measurements are readily available. This is the case for the high-order UAV system under study. An augmented closed-loop dynamic model is constructed using observer gains and the estimated states of the system. One can extend the TS system architecture of the continuous dynamic system to include the fuzzy observer rules. The pth fuzzy observer rule is represented as follows:

If v is V_p then

$$\dot{\hat{\boldsymbol{x}}}_{v_p}(t) = A_{v_p} \hat{\boldsymbol{x}}(t) + B_{v_p} u(t) + L_{v_p} [\boldsymbol{y}(t) - \hat{\boldsymbol{y}}(t)] \tag{19}$$

$$\hat{\boldsymbol{y}}_{v_p}(t) = C_{v_p} \hat{\boldsymbol{x}}(t) \tag{20}$$

where L_{v_p} is the observer gain matrix whose construction is described in the next section and $\hat{\boldsymbol{x}}(t)$, the fuzzy observer, is the vector of estimated system states. In the presence of the fuzzy observer, the fuzzy controller takes on the following form:

$$u(t) = -\sum_{p=1}^{R} \xi_p(v^d) K_p \hat{\boldsymbol{x}}(t) \tag{21}$$

The fuzzy observer for a fixed exogenous input velocity v^d is represented as the weighted sum of R fuzzy observer rules,

$$\dot{\hat{\boldsymbol{x}}}(t) = \sum_{p=1}^{R} \xi_p(v^d) \{ A_p \hat{\boldsymbol{x}}(t) + B_p u(t) + L_p [\boldsymbol{y}(t) - \hat{\boldsymbol{y}}(t)] \} \tag{22}$$

$$\hat{\boldsymbol{y}}(t) = \sum_{p=1}^{R} \xi_p(v^d) C_p \hat{\boldsymbol{x}}(t) \tag{23}$$

where $\xi_p(v^d)$ is the normalized fuzzy membership function for the pth fuzzy rule.

Combining the fuzzy control law (21) and the fuzzy observer equations (22) and (23), and denoting the state estimation error by $e(t) = \boldsymbol{x}(t) - \hat{\boldsymbol{x}}(t)$, we obtain the following closed-loop augmented system representation[7]:

$$\dot{\boldsymbol{x}}(t) = \sum_{i=1}^{R} \sum_{j=1}^{R} \xi_i(v^d) \xi_j(v^d) \{ (A_i - B_i K_j) \boldsymbol{x}(t) + B_i K_j \boldsymbol{e}(t) \} \tag{24}$$

$$\dot{\boldsymbol{e}}(t) = \sum_{i=1}^{R} \sum_{j=1}^{R} \xi_i(v^d) \xi_j(v^d) \{ A_i - L_i C_j \} \boldsymbol{e}(t) \} \tag{25}$$

When the control law (21) is substituted into the open-loop equation (6), the plant equation with feedback is represented as

$$\begin{aligned} \dot{\boldsymbol{x}}(t) &= A^d \boldsymbol{x}(t) - B^d K^d \hat{\boldsymbol{x}}(t) \\ &= A^d \boldsymbol{x}(t) - B^d K^d (\boldsymbol{x} - \boldsymbol{e})(t) \\ &= A^d \boldsymbol{x}(t) - B^d K^d \boldsymbol{x}(t) + B^d K^d \boldsymbol{e}(t) \end{aligned} \tag{26}$$

where A^d, B^d, and K^d denote the interpolation formulas (8), (9), and (17), respectively.

The augmented system can be expressed in equivalent computational matrix form as

$$\dot{\boldsymbol{x}}_a(t) = \sum_{i=1}^{R} \sum_{j=1}^{R} \xi_i(v^d) \xi_j(v^d) G_{ij} \boldsymbol{x}_a(t) \tag{27}$$

where

$$\boldsymbol{x}_a(t) = \begin{bmatrix} \boldsymbol{x}(t) \\ \boldsymbol{e}(t) \end{bmatrix} \tag{28}$$

$$G_{ij} = \begin{bmatrix} A_i - B_i K_j & B_i K_j \\ 0 & A_i - L_i C_j \end{bmatrix} \tag{29}$$

When interpolation formulas are used, the augmented computational matrix form becomes

$$\dot{\boldsymbol{x}}_a = \begin{bmatrix} \dot{\boldsymbol{x}}(t) \\ \dot{\boldsymbol{e}}(t) \end{bmatrix} = \begin{bmatrix} A^d - B^d K^d & B^d K^d \\ 0 & A^d - L^d C^d \end{bmatrix} \cdot \begin{bmatrix} \boldsymbol{x}(t) \\ \boldsymbol{e}(t) \end{bmatrix} \tag{30}$$

where the interpolated observer gain L^d is defined as

$$L^d = \sum_{p=1}^{R} \xi_p(v^d) L_p \tag{31}$$

The system of equations (30) is used in the simulations of the FGS closed-loop system described in this study. This system specifies the approximate system matrices (A^d, B^d, C^d) derived using interpolation formulas for a fixed velocity v^d. Numerical simulations verify the stabilization of the augmented closed-loop system, using fuzzy gains K^d and L^d, for both approximate system matrices and LTI matrices (A, B, C) specified at velocity v^d.

When interpolation formulas are used, Eqs. (21–23) can be expressed in a manner equivalent to Eq. (30):

$$\dot{\boldsymbol{x}}(t) = A^d\boldsymbol{x} - B^dK^d\hat{\boldsymbol{x}}(t) \tag{32}$$

$$\dot{\hat{\boldsymbol{x}}}(t) = L^d\boldsymbol{y}(t) + (A^d - B^dK^d - L^dC^d)\hat{\boldsymbol{x}}(t) \tag{33}$$

$$u = -K^d\hat{\boldsymbol{x}}(t) \tag{34}$$

Equations (33) and (34) describe a fuzzy regulator that serves as an observer-based feedback controller that is denoted by

$$u = \mathcal{F}(s)\boldsymbol{y} \tag{35}$$

where the fuzzy transfer function has the following form:

$$\mathcal{F}(s) = -K^d(sI - A^d + B^dK^d + L^dC^d)^{-1}L^d \tag{36}$$

The fuzzy regulator $\mathcal{F}$(s) can be computed using MATLAB's reg command. Connecting the regulator with positive feedback to the approximate plant dynamics produces an augmented closed-loop system with the equivalent dynamics of Eq. (30). The fuzzy regulator equations (33) and (34) can be adapted using difference equations for real-time applications. The input to the regulator is the vector of measured accelerometer sensor readings $\boldsymbol{y}$ and the output, the control signal u, that is fed back to the plant. The linear time-invariant model of the plant (A, B, and C matrices) may not be known during real-time performance of the controller.

Construction of Fuzzy Gain Scheduler

Construction of the fuzzy gain scheduler (the extended TS fuzzy logic control system) requires the building of the fuzzy sets V_p and the construction of the gain schedule. The gain schedule can be viewed as a table lookup of gains for interpolation between nominal operating conditions.

Construction of Fuzzy Sets

The first step in the construction of the gain scheduler requires the building of the fuzzy sets the typical values of which represent the nominal velocities. A fuzzy set V_p represents the pth nominal velocity and comprises the sole premise condition of three fuzzy rules: a system rule (3) and (4), controller rule (12), and observer rule (19) and (20). For the UAV model described in this study, the velocity range between 20 and 95 m/s is subdivided into a one-dimensional grid that consists of 16 nominal operating conditions. The nominal values of velocity in the stable operating region are contained in the set

$$V_s = \{20, 25, 30, 35, 40, 45, 50, 57.5\}$$

The nominal values in the unstable operating region are contained in the set

$$V_u = \{60, 65, 70, 75, 80, 85, 90, 95\}$$

The set $V_t = \{57.5, 60\}$ overlaps with V_s and V_u. The interval [57.5 60] (meters per second) is a transitionally weakly stable/unstable operating region. On this interval, velocities move monotonically from weakly stable to unstable. Unstable behavior begins to occur at $V_F \approx 59$ m/s.

Fuzzy sets are constructed along the velocity range as overlapping triangular membership functions. Each fuzzy membership function is piecewise continuous with a range belonging to the interval [0 1]. The typical value of a fuzzy set is the nominal velocity located along the base of its respective operating region. The shapes of the fuzzy velocity sets are unimodal and normal.[24] By convention, a fuzzy set is normal when its typical value takes on the membership function value 1; the set is unimodal when the typical value is a single discrete value and all other points in the set's operating range take on membership function values less than 1.

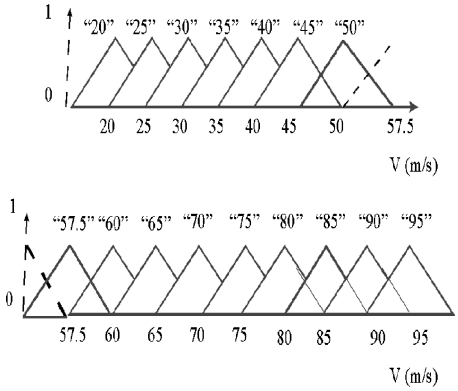

Fig. 4 Fuzzy triangular membership functions.

Figure 4 illustrates the fuzzy triangular membership functions. Linguistic labels "50," "57.5," . . . ,"95" describe the typical values assigned to their respective fuzzy sets. The shapes and number of fuzzy sets (corresponding to nominal velocities) were fine tuned to guarantee numerical stability of augmented closed-loop systems. The fuzzy sets "50," "57.5," and "60" are skewed triangular with a base of 12.5, 10, and 7.5 m/s, respectively; the remaining fuzzy sets are symmetric triangular membership functions with bases of 10 m/s.

Table 2 lists several of the normalized rule firings [$\xi_p(v^d)$, for fuzzy rule p] for fixed velocities over the transitionally weakly stable/unstable and unstable operating regions. Table 2 illustrates the uniform distribution of weighted rule firings. Over each fuzzy rule set, fixed nominal velocities activate one fuzzy rule with a weighted rule firing of 1. All other fixed velocities activate two weighted rule firings for each of the three fuzzy rule sets. Rule firings for the flutter speeds 59, 76.25, and 78 m/s are also shown in Table 2.

Construction of Gain Schedule

The UAV system is represented by a set of 16 nominal LTI plant models, P20 (20 m/s); P25 (25 m/s), . . . , P50 (50 m/s); P57p5 (57.5 m/s); P60 (60 m/s); P65 (65 m/s), . . . ; and P95 (maximum speed 95 m/s). The pth nominal LTI state-space model consists of three matrices: the open-loop ASE plant matrix $A_p^{39\times 39}$, the control vector $\boldsymbol{B}_p^{39\times 1}$, and the output matrix $C_p^{4\times 39}$. For the UAV system, $\boldsymbol{B}_p = \boldsymbol{B}$, a fixed real-valued column vector for $p = 1, \ldots, 16$. All elements of B are zero except for the nonzero 39th element. Both the plant matrix A_p and the output matrix C_p are real valued and parameterized by the exogenous velocity parameter. As the velocity varies, the matrix A_p becomes a smooth function of velocity and velocity squared.[19] The plant matrices were tested and validated for controllability (A_p, B_p) and observability (A_p, C_p). The first plant in the sequence of LTI models to have nonzero gains is plant P57p5. Fuzzy gain schedule design requires the construction of $\boldsymbol{K}_p^{39\times 1}$, $p = 8, \ldots, 16$, controller state feedback gain vectors and $L_p^{39\times 4}$, $p = 8, \ldots, 16$, observer gain matrices.

Construction of the state-feedback gain vectors, using MATLAB's Robust Control Toolbox,[18] proceeded as follows:

Step 1. LQG optimal control synthesis (MATLAB's lqg command) was used to compute an optimal controller to stabilize the most unstable operating plant P95. LQG minimizes the quadratic cost function

$$J(u) = \lim_{T\to\infty}\int_0^T [\boldsymbol{x}^T u^T] W \begin{bmatrix}\boldsymbol{x}(t)\\ u(t)\end{bmatrix} \mathrm{d}t, \qquad W = \begin{bmatrix} Q & N_c \\ N_c^T & R_c\end{bmatrix} \tag{37}$$

where the weighting parameters are

$$Q = 0 \times I_{39}, \qquad R_c = 1, \qquad N_c = 0_{39\times 1}$$

Table 2 Normalized weights

	Nominal operating velocities								
Fixed velocity	57.5	60	65	70	75	80	85	90	95
57.5	1	——	——	——	——	——	——	——	——
59	0.4	0.6	——	——	——	——	——	——	——
62	——	0.6	0.4	——	——	——	——	——	——
62.5	——	0.5	0.5	——	——	——	——	——	——
76.25	——	——	——	——	0.75	0.25	——	——	——
78	——	——	——	——	0.4	0.6	——	——	——
82.5	——	——	——	——	——	0.5	0.5	——	——
86.25	——	——	——	——	——	——	0.75	0.25	——
88	——	——	——	——	——	——	0.4	0.6	——
95	——	——	——	——	——	——	——	——	1

The real symmetric weighting matrices Q, N_c, and R_c are user specified and define the required tradeoff between regulation performance [how fast $\boldsymbol{x}(t)$ converges to zero] and control effort. For the 39th-order UAV system, minimization of the cost function $J(u)$ required the choice of weighting matrices that minimized the input control signal. Minimization of the cost function $J(u)$ is subject to the plant P95 equations

$$\dot{\boldsymbol{x}} = \left(A_{v_p=95}\right)\boldsymbol{x} + Bu + v \tag{38}$$

$$\boldsymbol{y} = \left(C_{v_p=95}\right)\boldsymbol{x} + \theta \tag{39}$$

V_f is the noise cross-correlation function,

$$E\left\{\begin{matrix} w(t) \\ \theta(\tau) \end{matrix}\right\}[w(t) \quad \theta(\tau)] = V_f\delta(t-\tau), \qquad V_f = \begin{bmatrix} \Xi & N_f \\ N_f^T & \Theta \end{bmatrix} \tag{40}$$

where $\Xi = I_{39}$, $N_f = 0_{39\times 4}$, and $\Theta = I_4$. Noise correlation matrices N_c and N_f were set to zero because noise models were not used in this investigation. LQG was implemented with a PDS[11] of $\alpha = 5.5$. This guarantees that all poles of the nominal closed-loop system have real parts that are less than $-\alpha$. The outputs of step 1 consist of the state feedback gain vector $\boldsymbol{K}_{v_p=95}$ for plant P95 and its corresponding poles that stabilized the closed-loop system $\dot{\boldsymbol{x}} = (A_{v_p=95} - B \times \boldsymbol{K}_{v_p=95})\boldsymbol{x}(t)$.

Step 2. By the use of the highest velocity stabilizing poles of step 1 and MATLAB's pole placement command, state feedback gains were constructed for the eight remaining nominal plant models on the interval [57.5 90] (meters per seconds). A fixed set of stabilizing poles facilitates the fuzzy interpolation of plant models and their fuzzy approximations at velocities between nominal operating conditions. Effective gain schedule design requires that the eigenvalues vary slowly and continuously between nominal velocities. The eigenvalues vary continuously as a function of the elements of the plant matrices A_p (Ref. 25) and as a function of flight velocity v.

Step 3. For the open-loop stable operating region between 20 and 50 m/s, gain scheduling is not required for feedback regulation, and the system is left as is. State feedback gains $K_p \equiv 0$, $p = 1, \ldots, 7$.

Step 4. The nine observer gain matrices, L_p, $p = 8, \ldots, 16$ were constructed using LQG synthesis with PDS $\alpha = 5.5$, at each nominal operating condition between 57.5 and 95 m/s.

Table 3 shows the least stable open and fuzzy gain scheduled closed-loop poles for the 16 nominal plant models. In the stable nominal operating region between plants P20 and P57p5, flutter mode 5 produces the least stable eigenvalues. Between nominal plants P60 and P75, flutter mode 7 produces the largest unstable eigenvalues. Between P80 and P95, the largest unstable eigenvalues occur for flutter mode 6. The least stable closed-loop FGS poles of plant P95 are maintained as the least stable closed-loop poles for plants, P57p5 (57.5 m/s), P60 (60 m/s), ..., P95 (95 m/s). The number of nominal gains required for effective gain scheduling was $\mathcal{O}(n)$, where n was the number of required gain scheduled nominal operating conditions.

The construction of continuous gains has been shown to be effective in preventing the occurrence of spikes, in the feedback control signal, due to switching between velocities while the gain scheduler is operating in real-time.[26] Reference 14 contains the proof of the following continuity property, which is a consequence of the fuzzy gain schedule construction and fuzzy gain interpolation as presented in this study:

Continuity property of fuzzy gains. The interpolated state feedback gain vector $\boldsymbol{K}^d(v)$ and the interpolated observer feedback matrix $L^d(v)$ are continuous piecewise smooth functions of v over the entire velocity envelope.

Table 3 Nominal plant characteristics 20–95 m/s[a]

Plant model	Open-loop stable	Mode	Closed-loop FGS
P20	$-0.63985 \pm 63.355i$	5	——
P25	$-0.64140 \pm 63.351i$	5	——
P30	$-0.64267 \pm 63.345i$	5	——
P35	$-0.64319 \pm 63.335i$	5	——
P40	$-0.64240 \pm 63.322i$	5	——
P45	$-0.63947 \pm 63.304i$	5	——
P50	$-0.63290 \pm 63.279i$	5	——
P57p5	$-0.60857 \pm 63.221i$	5	$-7.0371 \pm 324.78i$
P60	$0.526 \pm 108.17i$	7	$-7.0371 \pm 324.78i$
P65	$2.375 \pm 104.72i$	7	$-7.0371 \pm 324.78i$
P70	$2.962 \pm 100.97i$	7	$-7.0371 \pm 324.78i$
P75	$1.436 \pm 96.846i$	7	$-7.0371 \pm 324.78i$
P80	$5.163 \pm 75.922i$	6	$-7.0371 \pm 324.78i$
P85	$13.721 \pm 70.454i$	6	$-7.0371 \pm 324.78i$
P90	$20.637 \pm 65.649i$	6	$-7.0371 \pm 324.78i$
P95	$26.558 \pm 60.878i$	6	$-7.0371 \pm 324.78i$

[a]Least-stable/most-unstable eigenvalues.

Simulations

Numerical simulations describe the behavior of and verify the stabilization of augmented closed-loop systems. Simulations measure the responses to a 1000-V control pulse input command. As noted in Table 3, nominal plant models with velocities between 20 and 55 m/s were assigned zero gains and ran as open-loop stable systems. Augmented closed-loop systems are computed using three types of state-space descriptions. The first consists of approximate state-space models derived through FGS interpolation of nominal plant matrices as described in Eq. (30); the second consists of augmented closed-loop systems that combine LTI state-space models derived through rational approximations with FGS scheduled gains. A third set of augmented closed-loop systems consists of fuzzy regulator equations that are combined with LTI plant models. Numerical simulations also describe control effort as a function of observer error.

Comparison of FGS and LTI Models

FGS directs the augmented closed-loop system behavior on the velocity envelope that extends from 57.5 m/s to the maximum speed 95 m/s. LTI plant models were parameterized by velocities 1 m/s apart and by midpoint velocities between nominal operating conditions. Numerical simulations of the FGS algorithm verify the stability of the augmented closed-loop systems. In each case, when the

Table 4 Comparison of FGS approximate and LTI models[a]

Velocity, m/s	LTI (A, C)	FGS (A^d, C^d)	$\|A - A^d\|_2$	$\|C - C^d\|_2$
59	$-7.089 \pm 324.75i$	$-7.092 \pm 324.75i$	21.796	16.709
76.25	$-5.6211 \pm 102.22i$	$-5.6853 \pm 102.36i$	68.1	52.22
78	$-4.1527 \pm 104.39i$	$-4.2284 \pm 104.49i$	87.2	66.84

[a]Least-stable eigenvalues ($\alpha = 5.5$).

augmented closed-loop FGS model with interpolated A^d and C^d matrices and fixed input coefficient matrix B of Eq. (30) is stabilized, it follows that the augmented closed-loop LTI model

$$\dot{\boldsymbol{x}}_a = \begin{bmatrix} \dot{\boldsymbol{x}}(t) \\ \dot{\boldsymbol{e}}(t) \end{bmatrix} = \begin{bmatrix} A - BK^d & BK^d \\ 0 & A - L^dC \end{bmatrix} \cdot \begin{bmatrix} \boldsymbol{x}(t) \\ \boldsymbol{e}(t) \end{bmatrix} \tag{41}$$

with known coefficient matrices A, B, and C and interpolated gains K^d and L^d is also stabilized.

Table 4 presents a comparison, in terms of least-stable eigenvalues and two-norm differences, of approximate augmented closed-loop models produced by the FGS algorithm and their augmented closed-loop LTI counterparts. For both models, the augmented closed-loop systems are constructed with the interpolated FGS gains. The two-norm matrix, $\|A^d - A\|_2$ ($\|C^d - C\|_2$), which measures the distance between approximate A^d (C^d) and actual LTI coefficient matrix A (C) is defined as the singular value of $A^d - A$ ($C^d - C$) (Ref. 27). The comparison made in Table 4 demonstrates the robust performance of the fuzzy gains K^d and L^d when applied to both approximate and known plant models over the interval [57.5 95] (meters per second). FGS stabilized the augmented closed-loop systems (30) and (41) for two-norm differences of the (A, A^d) and (C, C^d) matrices, respectively, on the order $\mathcal{O}(10^2)$.

Stability Criteria for Fuzzy Regulator–LTI Equations

Numerical simulations were conducted over the range of velocities 57.5–95 m/s using plant equation (32) and the fuzzy regulator equations (33) and (34), with stabilization results comparable with those reported in Table 4 for matrix equations (30) and (41). Successful stabilization was also achieved when known matrices A and C were substituted for their approximate matrix counterparts (A^d, C^d) in Eqs. (32) and (33).

Numerical simulations, at nonnominal operating conditions, were also used to deduce performance criteria in the case where fuzzy regulator equations (33) and (34), using approximate (A^d, C^d, K^d, L^d) matrices, were connected using positive feedback to plant equation (32) with known LTI plant models (A, C) and measurable output vector $\boldsymbol{y}$. The augmented closed-loop system takes the matrix equation form

$$\dot{\boldsymbol{x}}_a = \begin{bmatrix} \dot{\boldsymbol{x}}(t) \\ \dot{\boldsymbol{e}}(t) \end{bmatrix} = \begin{bmatrix} A - BK^d & BK^d \\ (A - A^d) + L^d(C^d - C) & A^d - L^dC^d \end{bmatrix} \cdot \begin{bmatrix} \boldsymbol{x}(t) \\ \boldsymbol{e}(t) \end{bmatrix} \tag{42}$$

The matrix equation (42) does not satisfy the separation principle at nonnominal operating conditions for which $(A - A^d) + L^d(C^d - C)$ is nonzero.[27] Simulations were run on different nominal velocity grid configurations to determine stability bounds of two-norm differences for (A, A^d) and (C, C^d), respectively. Stability was achieved for all plants operating at velocities greater or equal to 57.5 m/s for nominal velocity grids, as in Fig. 4, that produced two-norm differences on the order $\mathcal{O}(10^2)$. Grid spacings that produced two-norm differences on the order $\mathcal{O}(10^3)$ produced unstable augmented closed-loop fuzzy regulator–LTI equations (42).

FGS System Behavior

Figure 5 shows the closed-loop FGS system response to a 1000-V pulse input command at flutter onset speeds 59, 76.25, and 78 m/s. Over the entire unstable region, the average minimum settling time was 0.2 s, occurring at $Y(2)$, the second accelerometer reading. The average maximum settling time was 0.4 s, occurring at $Y(1)$, the first accelerometer reading. Linear analysis of the augmented closed-loop models reveals right-hand-side zeros indicating nonminium phase behavior in both open-loop unstable and closed-loop stable systems.

Table 5 Flutter mode characteristics

	FGS open		FGS closed	
Mode V_F, m/s	ζ	ω, Hz	ζ	ω, Hz
7 (59)	−0.0002	17.33	0.079	15.56
5 (76.25)	−0.00005	10.04	0.13	10.25
6 (78)	−0.014	12.43	0.93	31.9

Table 6 Control effort (volts) vs observer error

Velocity, m/s	$e(0) = 0$	$e(0) = 0.00001$	$e(0) = 0.0001$
59	−1087.9	−820.65	3350.7
76.25	−900.9	−1173.7	−4462.3
78	−869	−1077.6	−3755.8
85	−697.9	−718.35	−1457.6
95	−352	−288.89	−569.84

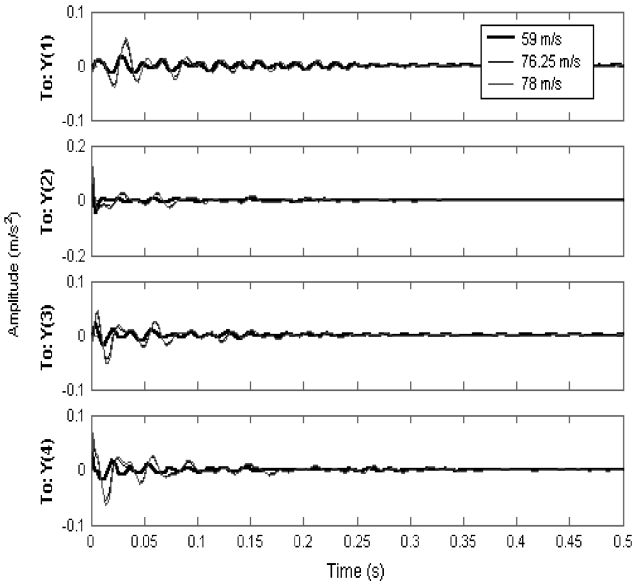

Fig. 5 FGS closed-loop system response at $v \in \{59,76.25,78\}$ m/s.

Table 5 compares the damping ratios and the frequency responses of the fuzzy interpolated open-loop (FGS-open) flutter modes described in Table 1 with the FGS closed-loop response.

FGS Control Effort

This section describes the control effort in terms of magnitude (volts) and observer error for the FGS system response to a 1000-V control pulse input. Within the scope of this investigation, control effort is expressed in terms of voltage. As shown in Ref. 20 (p. 316), PZT patch strains are proportional to control surface deflection voltage. Table 2 of Ref. 20 indicates the coefficients of proportionality for PZT patches in terms of microstrains for an input voltage of 1000 V. The allowable limits of PZT strain are within a control surface deflection of ±1000 V.

The performance of the interpolated fuzzy observers, $\hat{x}_1, \ldots, \hat{x}_{39}$, is dependent on the initial conditions as reflected in the observer error $\boldsymbol{e}(0) = \boldsymbol{x}(0) - \hat{\boldsymbol{x}}(0)$. Reported statistics are based on a simulation time frame, $T = 1$ s. The root mean square observer error (RMSE) is defined as $\|e(t)\|_2/39$, where 39 is the number of observer states and $\| \ \|_2$ is the Euclidean vector norm.

Table 6 shows the relationship between peak control effort (volts) and observer error at the flutter onset velocities 59, 76.25, and 78 m/s, and at 85 and 95 m/s. For the velocities in Table 6, FGS produces a median RMSE on the order $\mathcal{O}(1.5 \times 10^{-6})$ for $|e(0)| = 1 \times 10^{-5}$ and median RMSE on the order $\mathcal{O}(1.5 \times 10^{-5})$ for $|e(0)| = 1 \times 10^{-4}$. Here, $\mu_{\text{RMSE}} \approx 5 \times 10^{-5}$ for $|e(0)| = 1 \times 10^{-5}$ and $\mu_{\text{RMSE}} \approx 4 \times 10^{-4}$ for $|e(0)| = 1 \times 10^{-4}$. Simulations indicate that control effort magnitude tends to decrease with increase in velocity. This result is expected for gain construction based on highest velocity closed-loop poles.

Conclusions

The FGS algorithm performed as a global linear controller, given the underlying assumption that the exogenous parameter flight velocity was frozen in time. The novelty of this method of control is in the application of fuzzy interpolation to active flutter suppression in high-order nonminimum phase UAV systems. The flexibility of fuzzy interpolation enabled the construction of the interpolated gain vectors as continuous functions of velocity and permitted the nonlinear interpolation of velocity regions where the system behavior shifts from stable to unstable. Numerical simulations demonstrated the robustness of the FGS algorithm in its ability to stabilize system behavior over the weakly stable and unstable velocity range. Two-norm difference computations determined the stability bounds for three different state-space realizations of the fuzzy gain scheduled closed-loop systems. The FGS algorithm has been successfully applied to several generic high-order nonminimum phase UAV models. Numerical simulations of fuzzy regulator equations indicate the applicability of the FGS algorithm to real-time environments. Simulations demonstrate the effect of initial observer error on control effort and, thus, suggest the use of control signal saturation during real-time execution.

Acknowledgments

The first author was supported by the Center for Absorption in Science, Ministry of Immigrant Absorption, State of Israel. The authors also wish to acknowledge Boris Moulin for his insight and expertise in ASE modeling and analysis and Zvi Adin for his work in LQG/PDS regulator design.

References

[1]Waszak, M. R., "Robust Multivariable Flutter Suppression for Benchmark Active Control Technology Wind-Tunnel Model," *Journal of Guidance, Control, and Dynamics*, Vol. 24, No. 1, 2001, pp. 147–153.

[2]Scott, R. C., Hoadley, S. T., Wieseman, C. D., and Durham, M. H., "Benchmark Active Controls Technology Model Aerodynamic Data," *Journal of Guidance, Control, and Dynamics*, Vol. 23, No. 5, 2000, pp. 914–921.

[3]Mukhopadhyay, V., "Transonic Flutter Suppression Control Law Design and Wind-Tunnel Test Results," *Journal of Guidance, Control, and Dynamics*, Vol. 23, No. 5, 2000, pp. 930–937.

[4]Kelkar, A. G., and Joshi, S. M., "Passivity-Based Control with Application to Benchmark Active Controls Technology Wing," *Journal of Guidance, Control, and Dynamics*, Vol. 23, No. 5, 2000, pp. 938–947.

[5]Barker, J. R., and Balas, G. J., "Comparing Linear Parameter-Varying Gain-Scheduled Control Techniques for Active Flutter Suppression," *Journal of Guidance, Control, and Dynamics*, Vol. 23, No. 5, 2000, pp. 1030–1036.

[6]Adin, Z., Ben-Asher, J., Cohen, K., Moulin, B., and Weller, T., "Flutter Supression Using Linear Optimal and Fuzzy Logic Techniques," *Journal of Guidance, Control, and Dynamics*, Vol. 26, No. 1, 2003, pp. 173–177.

[7]Tanaka, K., and Wang, H. O., *Fuzzy Control Systems Design and Analysis: A Linear Matrix Inequality Approach*, Wiley, New York, 2001, Chap. 3.

[8]Applebaum, E., Ben-Asher, J. Z., and Weller, T., "Model Based Fuzzy Control For Flutter Suppression in Unmanned Aerial Vehicles," *Fourteenth International Conference on Adaptive Structures and Technologies (ICAST 2003)*, DEStech Publications, Inc., Lancaster, PA, 2004, pp. 444–457.

[9]Fujimori, A., and Tsunetomo, H.,"Gain-Scheduled Control Using Fuzzy Logic and Its Application to Flight Control," *Journal of Guidance, Control, and Dynamics*, Vol. 22, No. 1, 1999, pp. 175–178.

[10]Lin, C.-L., and Su, H.-W., "Adaptive Fuzzy Gain Scheduling in Guidance System Design," *Journal of Guidance, Control, and Dynamics*, Vol. 24, No. 4, 2001, pp. 683–692.

[11]Adin, Z., and Ben-Asher, J., "UAV's Flexible Modes Active Flutter Suppression," Faculty of Aerospace Engineering, Technion Aerospace Engineering Rept. 942, Technion—Israel Inst. of Technology, Haifa, Israel, June 2004.

[12]Adin, Z., and Ben-Asher, J.,"Updated UAV Aeroelastic Models-Stabilization Via LQG Regulators," Faculty of Aerospace Engineering, Technion Aerospace Engineering Rept. 890, Technion—Israel Inst. of Technology, Haifa, Israel, July 2002.

[13]Bernelli-Zazzera, F., Mantegazza, P., Mazzoni, G., and Rendina, M., "Active Flutter Suppression Using Recurrent Neural Networks," *Journal of Guidance, Control, and Dynamics*, Vol. 23, No. 6, 2000, pp. 1030–1036.

[14]Applebaum, E., Ben-Asher, J., and Weller, T., "Fuzzy Gain Scheduling Using Output Feedback for Flutter Suppression in Unmanned Aerial Vehicles with Piezoelectric Materials," Faculty of Aerospace Engineering, Technion Aerospace Engineering Rept. 943, Technion—Israel Inst. of Technology, Haifa, Israel, June 2004.

[15]Slotine, J.-J., and Li, W., *Applied Nonlinear Control*, Prentice–Hall, Englewood Cliffs, NJ, 1991, Chap. 6, pp. 207–278.

[16]Rusnak, I., "Control for Unstable Nonminimum Phase Uncertain Dynamic Vehicle," *IEEE Aerospace and Electronic Systems Magazine*, Vol. 32, No. 3, 1996, pp. 945–951.

[17]Grace, A., Laub, A., Little, J., and Thompson, C., "Control System Toolbox User's Guide," Ver. 4.2, Mathworks, Inc., Natick, MA, 1999.

[18]Chiang, R. Y., and Safanov, M. G., "Robust Control Toolbox User's Guide," Ver. 2, Mathworks, Inc., Natick, MA, 1996.

[19]Moulin, B., Feldgun, V., and Karpel, M., "Application of the State-Space Equation of the Integrated System in Stability and Response Analyses Including Sensitivity Evaluation, Part I: ASED Applications," Faculty of Aerospace Engineering, Technion Aerospace Engineering Rept. 899, Technion—Israel Inst. of Technology, Haifa, Israel, July 2002, Chaps. 4–6.

[20]Karpel, M., and Moulin, B., "Models for Aroservoelastic Analysis with Smart Structures," *Journal of Aircraft*, Vol. 41, No. 2, 2004, pp. 314–321.

[21]Karpel, M., "Time-Domain Aeroservoelastic Modeling Using Weighted Unsteady Aerodynamic Forces," *Journal of Guidance, Control, and Dynamics*, Vol. 13, No. 7, 1990, pp. 30–37.

[22]Idan, M., Karpel, M., and Moulin, B., "Aeroelastic Interaction Between Aircraft Structural and Control Design Schemes," *Journal of Guidance, Control, and Dynamics*, Vol. 22, No. 4, 1999, pp. 513–519.

[23]Takagi, T., and Sugeno, M., "Fuzzy Identification of Systems and Its Applications to Modeling and Control," *IEEE Transactions on Systems, Man, and Cybernetics*, Vol. 15, No. 1, 1985, pp. 116–132.

[24]Klir, G., St. Clair, U., and Yuan, B., *Fuzzy Set Theory: Foundations and Applications*, Prentice–Hall, Upper Saddle River, NJ, 1997, Chaps. 4 and 5, pp. 73–102.

[25]Horn, R., and Johnson, C., *Matrix Analysis*, Cambridge Univ. Press, New York, 1991, Chaps. 1 and 5.

[26]Stilwell, D. J., and Rugh, W. J., "Interpolation of Observer State Feedback Controllers for Gain Scheduling," *IEEE Transactions on Automatic Control*, Vol. 44, No. 6, 1999, pp. 1225–1229.

[27]Dorf, R., and Bishop, R., *Modern Control Systems*, Pearson Education, Upper Saddle River, NJ, 2005, Chap. 11, pp. 675–680.